# Electron Spin−Lattice Relaxation of the $S_0$ State of the Oxygen-Evolving Complex in Photosystem II and of Dinuclear Manganese Model Complexes†

L. V. Kulik,‡ W. Lubitz,* and J. Messinger*

*Max Planck Institute for Bioinorganic Chemistry, 45470 Mülheim/Ruhr, Germany*

*Received March 3, 2005; Revised Manuscript Received May 2, 2005*

ABSTRACT: The temperature dependence of the electron spin−lattice relaxation time $T_1$ was measured for the $S_0$ state of the oxygen-evolving complex (OEC) in photosystem II and for two dinuclear manganese model complexes by pulse EPR using the inversion−recovery method. For [Mn(III)Mn(IV)($\mu$-O)$_2$bipy$_4$]-$ClO_4$, the Raman relaxation process dominates at temperatures below 50 K. In contrast, Orbach type relaxation was found for [Mn(II)Mn(III)($\mu$-OH)($\mu$-piv)$_2$(Me$_3$tacn)$_2$]($ClO_4$)$_2$ between 4.3 and 9 K. For the latter complex, an energy separation of 24.7−28.0 cm$^{-1}$ between the ground and the first excited electronic state was determined. In the $S_0$ state of photosystem II, the $T_1$ relaxation times were measured in the range of 4.3−6.5 K. A comparison with the relaxation data (rate and pre-exponential factor) of the two model complexes and of the $S_2$ state of photosystem II indicates that the Orbach relaxation process is dominant for the $S_0$ state and that its first excited state lies 21.7 ± 0.4 cm$^{-1}$ above its ground state. The results are discussed with respect to the structure of the OEC in photosystem II.

Photosystem II (PSII)[1] is a unique enzyme that catalyzes the light-induced oxidation of water to molecular oxygen, protons, and bound electrons in higher plants, cyanobacteria, green, red, and brown algae, and diatoms. The water chemistry in PSII is catalyzed by a tetramanganese−oxygen−calcium cluster ($Mn_4O_xCa$) as the active site, which is termed the oxygen-evolving complex (OEC) (*1*−*3*). During the light-driven catalytic cycle (Kok cycle), the OEC passes through five redox states (S states, $S_0$−$S_4$). The oxygen is released during the $S_4 \rightarrow S_0$ transition (*4*). Despite numerous investigations using crystallography (*5*, *6*) and various types of spectroscopy (e.g., X-ray absorption, UV−vis, FTIR, and magnetic resonance) (*7*−*9*), the structures of the OEC in its different S states, the Mn oxidation states, and the mechanism of water splitting are still unknown.

EPR is the method of choice for a detailed study of the electronic structure of the OEC. Two of the S states ($S_0$ and $S_2$) have relatively strong multiline signals (MLS) in conventional perpendicular mode EPR (*10*−*13*). The complex structure of these spectra, which are produced by four coupled Mn nuclei (*14*), makes them extremely difficult to interpret. However, pulse EPR experiments such as electron spin−echo envelope modulation (ESEEM), electron−nuclear double resonance (ENDOR), and spin relaxation measurements were successfully used for the characterization of the $S_2$ state, and recently in part also for the $S_0$ state (*14*−*16*). ENDOR and ESEEM allow us to study the distribution of the electron spin density among the four Mn nuclei of the OEC and the interaction of their effective electron spin with nearby nuclei. In contrast, temperature-dependent electron spin−lattice relaxation time $T_1$ measurements allow in favorable cases the determination of the energy separation $\Delta$ between the ground and the first excited electronic states. This approach works well if the dominant process of the electron spin−lattice relaxation is of the Orbach type (*17*, *18*), i.e., involves phonon scattering via an excited electronic state that has a small energy separation $\Delta$ from its ground state in the paramagnetic species. At sufficiently low temperatures ($kT \ll \Delta$), the rate of the Orbach process depends exponentially on the inverse temperature

$$1/T_1 = A \exp(-\Delta/kT) \quad (1)$$

where $A$ is a pre-exponential factor, $k$ is the Boltzmann constant, and $T$ is the temperature.

Because of the complexity of the exchange coupling network of the $Mn_4O_xCa$ cluster, it is possible that there are several excited states with similar energies. If several excited states contribute to the spin−lattice relaxation rate, then eq 1 should be generalized:

$$1/T_1 = \sum_i A_i \exp(-\Delta_i/kT) \quad (2)$$

where index $i$ labels the excited states, $\Delta_i$ is the energy separation of the $i$th excited state from the ground state, and $A_i$ is the pre-exponential factor for the contribution of this

† This work was supported by the Max Planck Society and by the DFG (Me 1629/2-3). L.V.K. is thankful to the Alexander von Humboldt Foundation for financial support.

* To whom correspondence should be addressed. Phone: + 49-208-306-3865/-3614. Fax: + 49-208-306-3955. E-mail: lubitz@mpi-muelheim.mpg.de or messinger@mpi-muelheim.mpg.de.

‡ Permanent address: Institute of Chemical Kinetics and Combustion, Institutskaya 3, 630090 Novosibirsk, Russia.

[1] Abbreviations: OEC, oxygen-evolving complex; PSII, photosystem II; EPR, electron paramagnetic resonance; UV−vis, ultraviolet−visible; FTIR, Fourier transform infrared; MLS, multiline signal; ESE, electron spin−echo; ESEEM, electron spin−echo envelope modulation; ENDOR, electron−nuclear double resonance; CW, continuous wave; FSE, field-swept echo; FCCP, trifluoromethoxy carbonylcyanide phenylhydrazone; EDTA, ethylenediaminetetraacetic acid; ZFS, zero-field splitting.

10.1021/bi050411y CCC: $30.25 
Published on Web 06/11/2005

state to the total rate of the Orbach process. Several cases can be discussed. (i) If all pre-exponential factors are similar but the energy separations from the ground state differ substantially ($\Delta_i - \Delta_1 \gg kT$ for all $i \neq 1$, where $\Delta_1$ corresponds to the lowest excited state), then the contributions from the higher excited states are insignificant, and eq 2 reduces to eq 1 where $\Delta = \Delta_1$ and $A = A_1$. (ii) All $\Delta_i$ values are similar ($\Delta_i \approx \Delta_j \approx \Delta$, $|\Delta_i - \Delta_j| \ll kT$ for all $i$ and $j$). In this case, eq 2 again reduces to eq 1 with an effective pre-exponential factor $A = \sum_i A_i$. (iii) A more complex situation arises if $A_1$ is much smaller than the $A_i$ of a higher excited state. In this case, the significance of the relative contributions of these two different excited states to the Orbach process will vary with temperature. At sufficiently low temperatures, the contribution from the first excited state will be dominant, while at higher temperatures, the state with the larger $A_i$ will prevail. This situation can be easily detected because it will lead to a strong deviation of the temperature dependence of the relaxation rate from the simple exponential law given in eq 1. Such a deviation cannot be discerned from our data, and therefore, we assume in agreement with an earlier $T_1$ study on $[Fe_3S_4]^+$ clusters (*19*) that the most likely case, case i, is a good description for the $S_0$ state in PSII.

The value of $\Delta$ is highly important for the study of the structure of exchange-coupled clusters. For a binuclear cluster, knowledge of $\Delta$ is practically equivalent to the determination of the exchange coupling $J$, since $\Delta = 3J$ in such cases. Therefore, this parameter allows conclusions about the geometry of the complex, especially the approximate distance between the metal ions. When the nuclearity of the complex is greater than 2, the exchange coupling network becomes complicated. In such cases, the value of $\Delta$ can be used together with data from other methods (EPR, ENDOR, EXAFS, and magnetic susceptibility) to cross-check hypotheses about the unknown structure of the complex.

For a correct determination of $\Delta$, it is important to ensure that the Orbach process dominates the spin−lattice relaxation rate in the analyzed temperature range, because other relaxation processes such as Raman and direct relaxation can also contribute or even dominate the spin−lattice relaxation (*20*, *21*). The direct process is effective at only very low temperatures when the thermal energy $kT$ is close to the electron Zeeman energy. Therefore, this process can be neglected for experiments at X- and Q-band frequencies where $T > 4$ K, and only the Raman and Orbach processes will be discussed below. If a sufficiently large temperature range can be studied, the Raman and Orbach mechanisms can be distinguished from each other on the basis of their different temperature dependencies, which can be described in case of the Raman process by $1/T_1 \propto T^x$, with the exponent $x$ lying typically between 3 and 9.

Using this approach, it was concluded that the Orbach process dominates the relaxation of the $S_2$ state in the temperature range of 4.2−11 K, and an energy separation $\Delta$ of 36.5 ± 0.7 $cm^{-1}$ was deduced (*22*). Subsequently, it was reported that $\Delta$ may slightly depend on the $S_2$ state preparation, and that the magnetization recovery traces are biphasic for some preparations (*23*, *24*). Until now, no direct measurement of $T_1$ by pulse EPR has been reported for the $S_0$ state. Previously, the method of CW EPR microwave power saturation was employed to obtain indirect information about the relaxation processes in $S_0$. However, due to the intrinsic limitations of this approach, no clear distinction between the Raman mechanism and the Orbach mechanism could be made (*25*).

In this work, the temperature dependence of $T_1$ is obtained by the inversion−recovery method for the $S_0$ state of the OEC. For technical reasons, only a relatively small temperature range (4.3−6.5 K) can be studied with this sample. This makes it very difficult to distinguish between the Raman and Orbach processes on the basis of their different temperature dependencies. We therefore employ a novel approach and compare the $S_0$ data with $T_1$ times obtained for two well-characterized dinuclear manganese complexes: (i) "Bipy", [Mn(III)Mn(IV)($\mu$-O)$_2$bipy$_4$]$ClO_4$, where bipy is bipyridine (*26*), and (ii) "PivOH", [Mn(II)Mn(III)($\mu$-OH)-($\mu$-piv)$_2$(Me$_3$tacn)$_2$]($ClO_4$)$_2$, where piv is $(CH_3)_3CCO_2$ and tacn is 1,4,7-triazocyclononane (*27*, *28*). These two complexes were selected as models for this study, because they have different bridging motives between the two Mn centers. Consequently, the strength of the spin exchange coupling and the energy separation between ground and first excited states are markedly different; temperature-dependent magnetization measurements show $\Delta = 450$ $cm^{-1}$ and $\Delta = 25.5$ $cm^{-1}$ for Bipy and PivOH, respectively (*26*−*28*). In agreement with these previous results, (i) markedly different relaxation times are reported here for Bipy and PivOH, which can be clearly assigned to the Raman and Orbach processes, respectively, and (ii) a $\Delta$ of 24.7−28.0 $cm^{-1}$ is determined for PivOH. The comparison of the $T_1$ times of these model compounds with those of PSII in the $S_2$ and $S_0$ states indicates that the spin−lattice relaxation of the $S_0$ state is dominated by the Orbach mechanism and that the energy separation ($\Delta$) between the ground and first excited state(s) of the $S_0$ state is 21.7 ± 0.4 $cm^{-1}$.

## MATERIALS AND METHODS

*Pulse EPR Spectroscopy.* The experiments were performed using a Bruker Elexsys-580 Q-band pulse EPR spectrometer, which was equipped with a home-built cylindrical resonator (*29*) and an Oxford ITC-5025 helium flow-temperature controller and CF935 cryostat. To record field-swept echo (FSE) EPR spectra, the two-pulse $\pi/2-\tau-\pi-\tau-$echo sequence was used (sequence 1), while the electron spin−lattice relaxation was measured by the inversion−recovery $\pi-t-\pi/2-\tau-\pi-\tau-$echo pulse sequence (sequence 2). In both cases, the lengths of the microwave $\pi/2$ and $\pi$ pulses were 32 and 64 ns, respectively, and the entire echo was integrated.

*Sample Preparation.* PSII membranes were prepared according to standard procedures (*30*) and washed several times after the Triton treatment for starch removal. $S_0$ state samples were prepared using the three-flash, FCCP protocol described previously (*11*). The samples were finally concentrated by centrifugation in Q-band EPR tubes to a chlorophyll concentration of ~25 mg/mL. On the basis of the size of the $S_2$ EPR multiline amplitude that can be induced by 200 K illumination in comparison to a control $S_2$ sample, the $S_0$ state population was determined to be 65 ± 5% (the rest being $S_1$). All samples contained 3% (v/v) methanol, 50 $\mu$M phenyl-*p*-benzoquinone, 1 mM EDTA, and 3 $\mu$M FCCP. For the subtraction of background signals, dark ($S_1$ state) control samples containing the same additions were used.

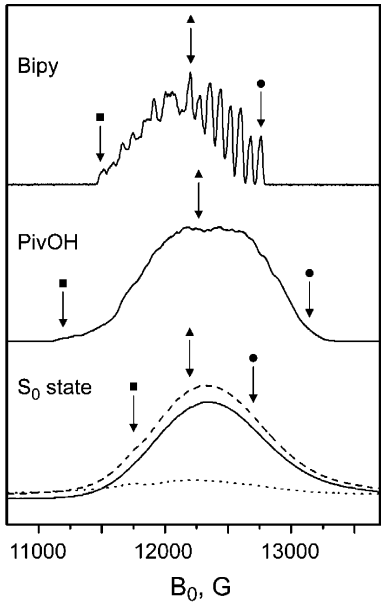


FIGURE 1: Field-swept echo Q-band EPR spectra (—) for Bipy, PivOH, and the pure $S_0$ state (light-minus-dark spectrum), (···) background signal measured with a dark ($S_1$ state) control sample, and (- - -) actual spectrum for the $S_0$ state sample (for details, see the text). Arrows and symbols indicate spectral positions for which inversion−recovery experiments were performed (see Figures 3, 4, and 6). Instrumental conditions: $T = 30$ K, $\nu_{MW} = 33.894$ GHz, $\tau = 300$ ns, and a repetition time of 10 ms for Bipy; $T = 4.5$ K, $\nu_{MW} = 33.986$ GHz, $\tau = 240$ ns, and a repetition time of 100 $\mu$s for PivOH; and $T = 4.3$ K, $\nu_{MW} = 33.862$ GHz, $\tau = 240$ ns, and a repetition time of 15 $\mu$s for the $S_0$ state.

Bipy and PivOH were prepared as previously described (*27*, *28*, *31*) and then dissolved in 1:3 mixtures of purified dry $CH_3CN$ and $CH_2Cl_2$ to give a final concentration of ~1 mM.

*Data Analysis.* Inversion−recovery traces were obtained by plotting the integrated echo intensities as a function of time $t$ of pulse sequence 2. For each trace, 1000 data points were collected over an appropriate time range. When a single-exponential approximation was adequate, the time constant of the exponential decay was assumed to be $T_1$. The dependence of the relaxation rate ($1/T_1$) on temperature $T$ is presented in two ways: (i) $\ln(1/T_1)$ versus $\ln(T)$ (Raman representation) and (ii) $\ln(1/T_1)$ versus $1/T$ (Orbach representation). In cases where a satisfactory linear fit to the data in the Orbach plot can be obtained, the slope equals $-\Delta/k$.

## RESULTS

Figure 1 presents the Q-band FSE EPR spectra of Bipy, PivOH, and the $S_0$ state. The pure $S_0$ EPR signal (solid line) is obtained from the experimental EPR spectrum of the $S_0$ sample (dashed line) by subtraction of a weak background signal (dotted line) that stems from oxidized cytochromes and possibly traces of free $Mn^{2+}$ (*32*). The background signal was measured separately in control samples that underwent the same treatment as the $S_0$ sample, with the exception of the three laser flashes used to generate the $S_0$ state. In these "dark" control samples, the OEC is in the dark-stable $S_1$ state that has no perpendicular mode EPR signal.

To optimize the signal intensities, $\tau$ (see sequences 1 and 2 in Materials and Methods) was varied for all complexes. In the case of Bipy and the $S_0$ state, the fine structures of the FSE EPR spectra are rather insensitive to variation in $\tau$. In contrast, the spectrum of PivOH shows a marked dependence on this parameter (only the trace for $\tau = 240$ ns is shown), which is most likely due to a magnetic field dependence of strong $^{14}N$ ESEEM of PivOH. Here this effect is not further explored, because $^{14}N$ ESEEM depends on nitrogen hyperfine and nuclear quadrupole interactions in a complicated way. On the other hand, it does not affect the $T_1$ measurements, which were performed at the magnetic field positions indicated by the arrows.

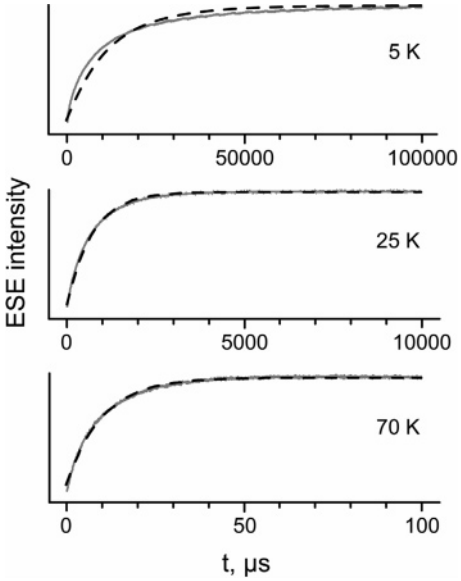


FIGURE 2: Inversion−recovery traces for Bipy (gray lines) at field positions $B_0 = 12\,200$ G (triangle in the top panel of Figure 1) and temperatures of 5, 25, and 70 K. Note the different time scales. Least-squares single-exponential fits are indicated by dashed lines. For further details, see the text.

For Bipy, the inversion−recovery traces obtained at three very different temperatures are displayed as solid gray lines in Figure 2 ($B_0 = 12\,200$ G). A dramatic increase in relaxation rate with temperature is observed (note the different time scales). The single-exponential fits (dashed lines) to the 25 and 70 K traces are in excellent agreement with the obtained data and give the following: $T_1 = 1380$ $\mu$s (25 K) and $T_1 = 11$ $\mu$s (70 K). Below 10−15 K, the recovery traces become nonexponential and nearly temperature-independent, with a characteristic time on the order of 100 ms (Figure 2, top).

Figure 3 shows the Orbach (left) and Raman (right) plots for Bipy between 15 and 80 K. Remarkably, almost identical results were obtained for the three field positions at which the experiments were performed (compare different symbols). The Orbach plot for Bipy deviates severely from linearity. In contrast, the Raman plot has a linear region with a slope $x$ of $3.94 \pm 0.07$ between 15 and 50 K (Figure 3, right). The obtained exponent is in the typical range for Raman processes ($3 < x < 9$). The deviation from this power dependence ($1/T_1 \propto T^x$) observed at higher temperatures ($T > 50$ K) may indicate an increasing contribution of the Orbach process. However, the $\Delta$ value for Bipy cannot be determined with good precision from our relaxation measurements.

The temperature dependence of $T_1$ was measured for PivOH using the same approach. However, due to the much

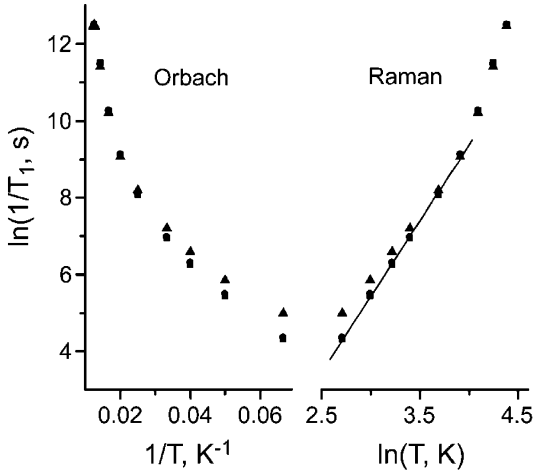


FIGURE 3: Temperature dependence of the spin−lattice relaxation rate for Bipy in Orbach (left) and Raman (right) representations. The measurements were performed at the following magnetic field positions: (■) $B_0$ = 11 480 G, (▲) $B_0$ = 12 200 G; and (●) $B_0$ = 12 760 G. A linear fit of the Raman plot for $B_0$ = 11 480 G (■) in the temperature range of 15−50 K is indicated with a straight line.

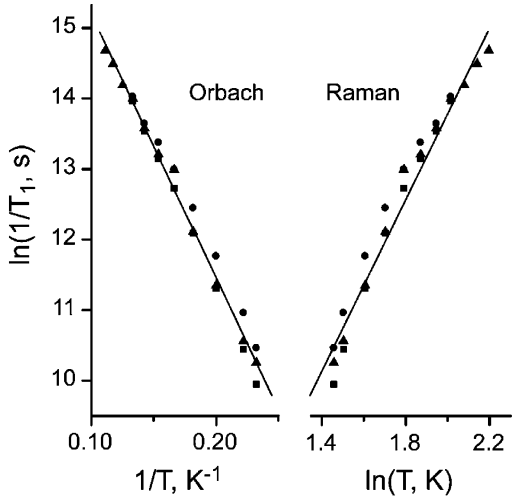


FIGURE 4: Temperature dependence of the spin−lattice relaxation rate of PivOH in Orbach and Raman representations. The measurements were performed at the following magnetic field positions: (■) $B_0$ = 11 170 G, (▲) $B_0$ = 12 200 G, and (●) $B_0$ = 13 250 G. The straight lines represent the linear fits of the Orbach and Raman plots for $B_0$ = 12 200 G (▲) in the temperature range of 4.3−9 K.

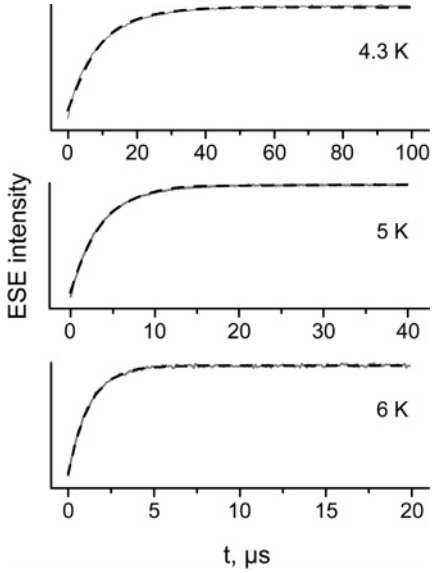


FIGURE 5: Inversion−recovery traces for the $S_0$ state (gray lines; light-minus-dark difference) at $B_0$ = 12 150 G (triangle in the bottom panel of Figure 1) and temperatures of 4.3, 5.0, and 6.0 K. Least-squares single-exponential fits are indicated by dashed lines. For further details, see the text.

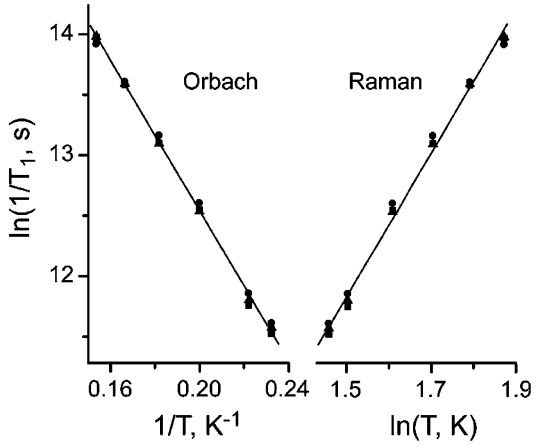


FIGURE 6: Temperature dependence of the spin−lattice relaxation rate of the $S_0$ state in Orbach and Raman representations. The measurements were performed at the following magnetic field positions: (■) $B_0$ = 11 750 G, (▲) $B_0$ = 12 150 G, and (●) $B_0$ = 12 700 G. The straight lines represent the linear fit of the Orbach and Raman plots for $B_0$ = 12 150 G (▲) in the temperature range of 4.3−6.5 K.

faster relaxation, the data could only be collected in the range of 4.3−8 K (field positions, 11 170 and 13 250 G) and between 4.3 and 9 K for the central field position (12 250 G). In contrast to those with Bipy, the recovery traces obtained with PivOH were all found to be monoexponential and to have at least 4 order of magnitude smaller $T_1$ times that range from 35.2 $\mu$s at 4.3 K to 0.42 $\mu$s at 9.0 K. Figure 4 presents the temperature dependence of the spin−lattice relaxation of PivOH at the three field positions in the form of Orbach and Raman plots. Despite the relatively small temperature range, it is obvious that the linear fit to the Orbach plot ($R$ = 0.998) agrees better with the data than the linear fit to the Raman plot ($R$ = 0.989), which shows a systematic curvature. From the Orbach plot, slightly different $\Delta$ values and pre-exponential factors are obtained for the three field positions: $\Delta$ = 28.0 ± 0.4 cm$^{-1}$ and $1/A$ = 4.1 ns for $B_0$ = 11 170 G (■); $\Delta$ = 26.1 ± 0.6 cm$^{-1}$ and $1/A$ = 6.1 ns for $B_0$ = 12 250 G (▲); and $\Delta$ = 24.7 ± 0.6 cm$^{-1}$ and $1/A$ = 7 ns for $B_0$ = 13 250 G (●).

The inversion−recovery traces of the pure $S_0$ state are obtained as the light-minus-dark difference (see above). Figure 5 shows these difference traces (solid gray lines) for three temperatures (4.3, 5.0, and 6.0 K at $B_0$ = 12 150 G). The single-exponential fits (dashes) provide satisfactory descriptions of the data and yield $T_1$ values between 9.4 $\mu$s (4.3 K) and 0.85 $\mu$s (6.5 K). At higher temperatures, no data could be obtained, because the echo signal from the $S_0$ state becomes too small to be measured reliably. Figure 6 shows the Orbach and Raman plots for the $S_0$ state. The very good agreement between the data sets measured at the three magnetic field positions (different symbols) supports our analysis. Both Orbach and Raman plots can be described reasonably well by linear fits (solid lines) with $R$-factors of

0.9995 and 0.9986, respectively. From the Orbach plot, $\Delta$ and $1/A$ values of $21.7 \pm 0.4$ cm$^{-1}$ and 7 ns, respectively, were determined for the $S_0$ state, while the fit to the Raman representation yields an $x$ value of $5.95 \pm 0.15$. A small systematic curvature similar to that seen with PivOH (Figure 4, right) may be discernible for the Raman plot of the $S_0$ state data.

## DISCUSSION

For a system with two antiferromagnetically coupled ions (exchange Hamiltonian $H_{ex} = -2JS_1S_2$) with an $S = {}^1/_2$ ground state and an $S = {}^3/_2$ first excited state, the energy splitting $\Delta$ between these states equals $3J$. This description provides a good approximation for Bipy, because the zero-field splitting (ZFS) of the Mn ions (usually on the order of several cm$^{-1}$) is small compared to the coupling constant $J$, which for this complex is $\sim$150 cm$^{-1}$ according to temperature-dependent magnetic susceptibility measurements (*26*). Since $\Delta = 3J = 450$ cm$^{-1}$ and this value is much larger than the thermal energy $kT$ at $T < 50$ K, this also explains why the contribution of the Orbach process to the relaxation rate is negligible for Bipy at low temperatures. Thus, only Raman and direct processes and spectral diffusion contribute to the recovery rate under these conditions. The nonexponentiality of the recovery traces and their virtual temperature independence below 10 to 15 K indicate that spectral diffusion becomes dominant under these conditions. Spin diffusion is an intermolecular process that involves mutual electron spin flip-flops, caused by dipolar interaction between Bipy molecules. This process is quasi-resonant and is known to have a weak temperature dependence (*33*). Thus, the actual $T_1$ relaxation caused by Raman and direct processes must be even slower than the apparent magnetization recovery time and is estimated to be hundreds of milliseconds or longer in the temperature range of 5−10 K.

At temperatures below 10 K, the magnetization recovery for PivOH (Figure 4) is $\sim$4 orders of magnitude faster than that measured for Bipy. Since both complexes have two Mn ions and were dissolved in the same solvents with a final concentration of 1 mM, the contributions from the Raman process, from the direct process, and from spectral diffusion should be comparable. The difference in the recovery rates can therefore only be explained by the appearance of an additional relaxation process for PivOH. This process is readily assigned to the Orbach process, since from temperature-dependent magnetic susceptibility measurements PivOH is known to have a low-lying excited state ($\Delta = 3J = 25.5$ cm$^{-1}$, if ZFS is neglected for the first excited state). The $\Delta$ values determined from the Orbach plot in Figure 4 (top) depend slightly on the magnetic field value and vary between 24.7 and 28.0 cm$^{-1}$. This excellent agreement confirms our analysis. The dependence of $\Delta$ on the spectral position is probably caused by the high orientation selection of the Q-band measurements: different magnetic field positions correspond to different orientations of the PivOH molecule with respect to this external magnetic field, which leads to a small variation of the $\Delta$ value by differences in the ZFS of the excited state.

The recovery traces for the $S_0$ state are independent of the spectral position. This is expected, since the high level of complexity of the $S_0$ EPR spectrum prevents orientation selection. In the small temperature range that is accessible for the $T_1$ study of the $S_0$ samples, both Raman and Orbach plots can be described well by linear fits. Although the fit to the Orbach plot has a slightly better $R$-factor and a small systematic curvature may be discernible in the Raman plot, it is very difficult in this case to unambiguously discriminate between the two processes using this type of analysis. Therefore, we also need to compare the absolute values of $T_1$ and of the pre-exponential factor with relaxation data of relevant model systems.

At identical temperatures (4.3 K), the $T_1$ value of the $S_0$ state is $\sim$4 times smaller than that of PivOH (Orbach process) but at least 4 orders of magnitude smaller than that of Bipy (Raman process). On the basis of this comparison, we suggest that the fast relaxation of the $S_0$ state is determined by the Orbach process. Further support for this assignment comes from the relaxation rate of the $S_2$ state. The $S_2$ state can be considered to be the best "model complex" for the $S_0$ state, since the protein environment and the structure of the $Mn_4O_xCa$ complex are very similar for these two states of the OEC (*34*, *35*). As shown previously, the relaxation of the $S_2$ state is governed by the Orbach process where $T_1 = 1.22$ ms at 4.2 K (*22*). This means that the contribution of the Raman process to the relaxation rate of the $S_2$ state is small; i.e., its rate must be several times slower. If we assume that the relaxation of the $S_0$ state ($T_1 = 9.3$ $\mu$s at 4.3 K) proceeds via the Raman process, this would imply that the rate of this process differs by more than 2 orders of magnitude between the $S_0$ and $S_2$ states, which is unlikely. We therefore conclude that the relaxation of the $S_0$ state most likely proceeds via the Orbach process.

This assignment is further supported by the close coincidence of the pre-exponential factors measured in this work for the $S_0$ state ($1/A = 7$ ns) and those determined for different forms of the $S_2$ state (*22*, *23*), which range typically from 5 to 30 ns. Interestingly, these values also agree very well with that measured in this work for PivOH (4.1−7 ns).

Our analysis deviates from conclusions reached previously by Styring and co-workers (*25*). On the basis of Curie plots and microwave power saturation studies of the $S_2$ and $S_0$ EPR multiline signals, these authors concluded that (i) the $S_0$ state has no thermally accessible excited state, (ii) the energy gap $\Delta$ is at least twice as large for $S_0$ as for $S_2$, and (iii) the $T_1$ relaxation in $S_0$ (and possibly also in $S_2$) occurs via the Raman process. These conclusions are based mainly on the Curie plot (unsaturated EPR multiline intensity vs inverse temperature) obtained by this group for the $S_0$ state. Taking into account (i) the small signal amplitude of the $S_0$ EPR multiline signal even under optimal conditions, (ii) the deviating reports for Curie plots for the much more intense $S_2$ EPR multiline signal, and (iii) the oversimplified interpretation of the Curie plots with the exchange Hamiltonian $H_{ex} = -2JS_1S_2$ [a two-spin instead of a four-spin system (*7*, *36*)], we consider these arguments to be nonconclusive. Interestingly, the disregarded Orbach plot of this previous study indicated $\Delta = 17 \pm 1$ cm$^{-1}$, which is in reasonable agreement with our result given the uncertainties of the power saturation method.

Due to the small difference in $\Delta$ values between PivOH and the $S_0$ state, it is tempting to assume that the $S_0$ state may also contain a Mn(II)Mn(III) dimer, with the other two Mn ions of the $Mn_4O_xCa$ cluster forming a strongly anti-

ferromagnetically coupled Mn(III,III) or Mn(IV,IV) dimer with $S = 0$. However, the fact that the $\Delta$ value of the $S_2$ state (33.8−39.7 $cm^{-1}$), which definitively does not contain Mn(II) (*37*), also matches that of PivOH shows that no conclusion about Mn oxidation states can be derived from such a comparison.

More important than the Mn oxidation states is the strength of the coupling between the Mn centers. The weak coupling in PivOH leads to a low-lying excited state, while the strong coupling by two $\mu$-oxo bridges in Bipy results in a large gap between the ground and first excited state. Taking into account the fact that all four Mn ions of the OEC are coupled (*14*), we found the $Mn_4O_xCa$ cluster may, independent of its oxidation state ($S_0$ or $S_2$), contain either (i) a mixed-valent Mn dimer (II,III or III,IV) weakly coupled to a homovalent Mn dimer (III,III or IV,IV), (ii) a linear mixed-valent trimer weakly coupled to a monomer (*15*), or (iii) a closed Mn trimer unit (plus a monomer) (*9*, *38*) with a low-lying excited state created by spin frustration and/or by the weak coupling to the monomer. These data will be used in combination with our recently obtained $^{55}$Mn ENDOR spectra (*14*) to find a satisfying description for the spin coupling network of the four Mn ions and to construct a model for the $Mn_4O_xCa$ cluster of the OEC.

## ACKNOWLEDGMENT

We are grateful to Dr. H. Hummel, Dr. T. Weyhermüller, and Prof. K. Wieghardt (MPI for Bioinorganic Chemistry, Mülheim/Ruhr, Germany) for providing compounds PivOH and Bipy.

## REFERENCES

1. Nugent, J. H. A. (1996) Oxygenic photosynthesis, *Eur. J. Biochem. 237*, 519−531.
2. Renger, G. (2004) Coupling of electron and proton transfer in oxidative water cleavage in photosynthesis, *Biochim. Biophys. Acta 1655*, 195−204.
3. Britt, R. D. (1996) in *Oxygenic Photosynthesis: The Light Reactions* (Ort, D. R., and Yocum, C. F., Eds.) pp 137−164, Kluwer Academic Publishers, Dordrecht, The Netherlands.
4. Kok, B., Forbush, B., and McGloin, M. (1970) Cooperation of charges in photosynthetic $O_2$ evolution, *Photochem. Photobiol. 11*, 457−476.
5. Ferreira, K. N., Iverson, T. M., Maghlaoui, K., Barber, J., and Iwata, S. (2004) Architecture of the photosynthetic oxygen-evolving center, *Science 303*, 1831−1838.
6. Biesiadka, J., Loll, B., Kern, J., Irrgang, K. D., and Zouni, A. (2004) Crystal structure of cyanobacterial photosystem II at 3.2 Å resolution: A closer look at the Mn-cluster, *Phys. Chem. Chem. Phys. 6*, 4733−4736.
7. Carell, T. G., Tyryshkin, A. M., and Dismukes, G. C. (2002) An evaluation of structural models for the photosynthetic water oxidizing complex derived from spectroscopic and X-ray diffraction signatures, *J. Biol. Inorg. Chem. 7*, 2−22.
8. McEvoy, J. P., and Brudvig, G. W. (2004) Structure-based mechanism of photosynthetic water oxidation, *Phys. Chem. Chem. Phys. 6*, 4754−4763.
9. Messinger, J. (2004) Evaluation of different mechanistic proposals for water oxidation in photosynthesis on the basis of $Mn_4O_xCa$ structures for the catalytic site and spectroscopic data, *Phys. Chem. Chem. Phys. 6*, 4764−4771.
10. Dismukes, G. C., and Siderer, Y. (1981) Intermediates of a polynuclear manganese cluster involved in photosynthetic oxidation of water, *Proc. Natl. Acad. Sci. U.S.A. 78*, 274−278.
11. Messinger, J., Robblee, J. H., Yu, W. O., Sauer, K., Yachandra, V. K., and Klein, M. P. (1997) The $S_0$ state of the oxygen evolving complex in photosystem II is paramagnetic: Detection of an EPR multiline signal, *J. Am. Chem. Soc. 119*, 11349−11350.
12. Messinger, J., Nugent, J. H. A., and Evans, M. C. W. (1997) Detection of an EPR multiline signal for the $S_0$* state in photosystem II, *Biochemistry 36*, 11055−11060.
13. Åhrling, K. A., Peterson, S., and Styring, S. (1997) An oscillating manganese electron paramagnetic resonance signal from the $S_0$ state of the oxygen evolving complex in photosystem II, *Biochemistry 36*, 13148−13152.
14. Kulik, L. V., Epel, B., Lubitz, W., and Messinger, J. (2005) $^{55}$Mn pulse ENDOR at 34 GHz of the $S_0$- and $S_2$-states of the oxygen evolving complex in photosystem II, *J. Am. Chem. Soc. 127*, 2392−2393.
15. Peloquin, J. M., Campbell, K. A., Randall, D. W., Evanchik, M. A., Pecoraro, V. L., Armstrong, W. H., and Britt, R. D. (2000) $^{55}$Mn ENDOR of the $S_2$-state multiline EPR signal of photosystem II: Implications on the structure of the tetranuclear Mn cluster, *J. Am. Chem. Soc. 122*, 10926−10942.
16. Britt, R. D., Campbell, K. A., Peloquin, J. M., Gilchrist, M. L., Aznar, C. P., Dicus, M. M., Robblee, J., and Messinger, J. (2004) Recent pulsed EPR studies of the photosystem II oxygen-evolving complex: Implications as to water oxidation mechanisms, *Biochim. Biophys. Acta 1655*, 158−171.
17. Orbach, R. (1961) Spin−lattice relaxation in rare-earth salts, *Proc. R. Soc. London, Ser. A 264*, 458−484.
18. Orbach, R. (1961) Spin−lattice relaxation in rare-earth salts: Field dependence of 2-phonon process, *Proc. R. Soc. London, Ser. A 264*, 485−495.
19. Telser, J., Lee, H. I., and Hoffman, B. M. (2000) Investigation of exchange couplings in $[Fe_3S_4]^+$ clusters by electron spin−lattice relaxation, *J. Biol. Inorg. Chem. 5*, 369−380.
20. Wagner, G. C., Colvin, J. T., Allen, J. P., and Stapleton, H. J. (1985) Fractal models of protein-structure, dynamics, and magnetic-relaxation, *J. Am. Chem. Soc. 107*, 5589−5594.
21. Schweiger, A. J. G. (2001) *Principles of Pulse Electron Paramagnetic Resonance*, Oxford University Presss, Oxford, U.K.
22. Lorigan, G. A., and Britt, R. D. (1994) Temperature-dependent pulsed electron-paramagnetic-resonance studies of the $S_2$ state multiline signal of the photosynthetic oxygen-evolving complex, *Biochemistry 33*, 12072−12076.
23. Lorigan, G. A., and Britt, R. D. (2000) Electron spin−lattice relaxation studies of different forms of the $S_2$ state multiline EPR signal of the photosystem II oxygen-evolving complex, *Photosynth. Res. 66*, 189−198.
24. Kodera, Y., Dzuba, S. A., Hara, H., and Kawamori, A. (1994) Distances from tyrosine $D^+$ to the manganese cluster and the acceptor iron in photosystem II as determined by selective hole-burning in EPR spectra, *Biochim. Biophys. Acta 1186*, 91−99.
25. Geijer, P., Peterson, S., Åhrling, K. A., Deak, Z., and Styring, S. (2001) Comparative studies of the $S_0$ and $S_2$ multiline electron paramagnetic resonance signals from the manganese cluster in photosystem II, *Biochim. Biophys. Acta 1503*, 83−95.
26. Cooper, S. R., Dismukes, G. C., Klein, M. P., and Calvin, M. (1978) Mixed-valence interactions in di-$\mu$-oxo bridged manganese complexes: Electron-paramagnetic resonance and magnetic-susceptibility studies, *J. Am. Chem. Soc. 100*, 7248−7252.
27. Hummel, H. (1998) Bioanorganische Modellverbindungen für die aktiven Zentren eisen- und manganhaltiger Metalloproteine, Ph.D. Thesis, Ruhr-Universität, Bochum, Germany.
28. Bossek, U., Hummel, H., Weyhermüller, T., Wieghardt, K., Russell, S., van der Wolf, L., and Kolb, U. (1996) The $[Mn_2(IV)(\mu\text{-}O)(\mu\text{-}PhBO_2)_2]^{2+}$ unit: A new structural model for manganese-containing metalloproteins, *Angew. Chem., Int. Ed. Engl. 35*, 1552−1554.
29. Sinnecker, S., Reijerse, E., Neese, F., and Lubitz, W. (2004) Hydrogen bond geometries from electron paramagnetic resonance and electron−nuclear double resonance parameters: Density functional study of quinone radical anion−solvent interactions, *J. Am. Chem. Soc. 126*, 3280−3290.
30. Berthold, D. A., Babcock, G. T., and Yocum, C. F. (1981) A highly resolved, oxygen-evolving photosystem II preparation from spinach thylakoid membranes, *FEBS Lett. 134*, 231−234.
31. Cooper, S. R., and Calvin, M. (1977) Mixed-valence interactions in di-$\mu$-oxo bridged manganese complexes, *J. Am. Chem. Soc. 99*, 6623−6630.
32. Mino, H., Kawamori, A., and Ono, T. (2000) Pulsed EPR studies of doublet signal and singlet-like signal in oriented $Ca^{2+}$-depleted PSII membranes: Location of the doublet signal center in PSII, *Biochemistry 39*, 11034−11040.
33. Borovykh, I. V., Kulik, L. V., Dzuba, S. A., and Hoff, A. J. (2001) Selective excitation in pulsed EPR of spin-correlated radical

pairs: Electron−electron interactions, zero-, single-, and double-quantum relaxation and spectral diffusion, *Chem. Phys. Lett. 338*, 173−179.

34. Robblee, J. H., Messinger, J., Cinco, R. M., McFarlane, K. L., Fernandez, C., Pizarro, S. A., Sauer, K., and Yachandra, V. K. (2002) The Mn cluster in the $S_0$ state of the oxygen evolving complex of photosystem II studied by EXAFS spectroscopy: Are there three di-$\mu$-oxo-bridged $Mn_2$ moieties in the tetranuclear Mn complex? *J. Am. Chem. Soc. 124*, 7459−7471.
35. Yachandra, V. K., Sauer, K., and Klein, M. P. (1996) Manganese cluster in photosynthesis: Where plants oxidize water to dioxygen, *Chem. Rev. 96*, 2927−2950.
36. Zheng, M., and Dismukes, G. C. (1996) Orbital configuration of the valence electrons, ligand field symmetry, and manganese oxidation states of the photosynthetic water oxidizing complex: Analysis of the $S_2$ state multiline EPR signals, *Inorg. Chem. 35*, 3307−3319.
37. Messinger, J., Robblee, J. H., Bergmann, U., Fernandez, C., Glatzel, P., Visser, H., Cinco, R. M., McFarlane, K. L., Bellacchio, E., Pizarro, S. A., Cramer, S. P., Sauer, K., Klein, M. P., and Yachandra, V. K. (2001) Absence of Mn centered oxidation in the $S_2$ to $S_3$ transition: Implications for the mechanism of photosynthetic water oxidation, *J. Am. Chem. Soc. 123*, 7804−7820.
38. Cinco, R. M., Robblee, J. H., Messinger, J., Fernandez, C., Holman, K. L. M., Sauer, K., and Yachandra, V. K. (2004) Orientation of calcium in the $Mn_4Ca$ cluster of the oxygen-evolving complex determined using polarized strontium EXAFS of photosystem II membranes, *Biochemistry 43*, 13271−13282.

BI050411Y